European Journal of Nuclear Medicine and Molecular Imaging (2022) 49:1030–1040
https://doi.org/10.1007/s00259-021-05486-x

ORIGINAL ARTICLE

^{68}Ga-labeled ODAP-Urea-based PSMA agents in prostate cancer: first-in-human imaging of an optimized agent

Xiaojiang Duan[1] · Zhen Cao[1] · Hua Zhu[2] · Chen Liu[2] · Xiaojun Zhang[3] · Jinming Zhang[3] · Ya'nan Ren[2] · Futao Liu[2] · Xuekang Cai[1] · Xiaoyi Guo[2] · Zhen Xi[4] · Martin G. Pomper[5] · Zhi Yang[2] · Yan Fan[1] · Xing Yang[1,6]

Received: 25 March 2021 / Accepted: 3 July 2021 / Published online: 28 August 2021

Abstract

Purpose Prostate-specific membrane antigen (PSMA) is a promising target for prostate cancer imaging and therapy. The most commonly used scaffold incorporates a glutamate-urea (Glu-Urea) function. We recently developed oxalyldiaminopropionic acid-urea (ODAP-Urea) PSMA ligands in an attempt to improve upon the pharmacokinetic properties of existing agents. Here, we report the synthesis of an optimized ^{68}Ga-labeled ODAP-Urea-based ligand, [^{68}Ga]Ga-P**137**, and first-in-human results.

Methods Twelve ODAP-Urea-based ligands were synthesized and radiolabeled with ^{68}Ga in high radiochemical yield and purity. Their PSMA inhibitory capacities were determined using the NAALADase assay. Radioligands were evaluated in mice-bearing 22Rv1 prostate tumors by microPET. Lead compound [^{68}Ga]Ga-P**137** was evaluated for stability, cell uptake, and biodistribution. PET imaging of [^{68}Ga]Ga-P**137** was performed in three patients head-to-head compared to [^{68}Ga]Ga-PSMA-617.

Results Ligands were synthesized in 11.1-44.4% yield and > 95% purity. They have high affinity to PSMA (K_i of 0.13 to 5.47 nM). [^{68}Ga]Ga-P**137** was stable and hydrophilic. [^{68}Ga]Ga-P**137** showed higher uptake than [^{68}Ga]Ga-PSMA-617 in tumor-bearing mice at 6.43 ± 0.98%IA/g vs 3.41 ± 1.31%IA/g at 60-min post-injection. In human studies, the normal organ biodistribution of [^{68}Ga]Ga-P**137** was grossly equivalent to that of [^{68}Ga]Ga-PSMA-617 except for within the urinary tract, in which [^{68}Ga]Ga-P**137** demonstrated lower uptake.

Conclusion The optimized ODAP-Urea-based ligand [^{68}Ga]Ga-P**137** can image PSMA in xenograft models and humans, with lower bladder accumulation to the Glu-Urea-based agent, [^{68}Ga]Ga-PSMA-617, in a preliminary, first-in-human study.

Trial registration ClinicalTrials.gov Identifier: NCT04560725, Registered 23 September 2020. https://clinicaltrials.gov/ct2/show/NCT04560725

Keywords Prostate-specific membrane antigen (PSMA) · Oxalyldiaminopropionic acid-urea (ODAP-Urea) ligand · Translational imaging · Prostate cancer

Introduction

Prostate cancer (PCa) is the second most frequent lethal cancer in men [1]. Imaging methods with high sensitivity and specificity are needed for accurate staging and other scenarios to manage patients with PCa [2]. Prostate-specific membrane antigen (PSMA) is an attractive target for radionuclide imaging and therapy of PCa [3–7]. Among PSMA-targeting agents, low-molecular-weight radioligands derived from its potent inhibitors have received worldwide attention. Recently, several such radiopharmaceuticals have reached clinical trials and have demonstrated high sensitivity and specificity for detecting PCa. Those agents include [^{18}F]DCFBC [8], [^{18}F]DCFPyL [9], [^{18}F]PSMA-1007 [10],

Xiaojiang Duan, Zhen Cao and Hua Zhu contribute equally to this work.

This article is part of the Topical Collection on Radiopharmacy

✉ Zhi Yang
pekyz@163.com

✉ Yan Fan
fanyan980618@sina.com; fanyan@bjmu.edu.cn

✉ Xing Yang
yangxing2017@bjmu.edu.cn

Extended author information available on the last page of the article

[^{68}Ga]Ga-PSMA-11 [11], [^{68}Ga]Ga-PSMA-617 [12, 13], and [^{68}Ga]Ga-PSMA I&T [14], among others. Despite the promise of these imaging agents, challenges such as high radiation dose to salivary glands and the kidneys and bladder remain, justifying further work to improve pharmacokinetics.

Nearly all low-molecular-weight imaging agents targeting PSMA have derived from a Glu-Urea-based targeting moiety. Among the non-Glu-Urea-based PSMA-targeting ligands, phosphonate/phosphoramidate and Glu-carbamate inhibitors have been developed from functional group tuning at the zinc-binding site of PSMA catalytic pocket [15, 16]. As an alternative, we recently reported a series of PSMA inhibitors based on the oxalyldiaminopropionic acid-urea (ODAP-Urea) scaffold, which represents one of very few examples modifying the glutamate-like moiety binding to the S1' sub-binding domain of PSMA with similar or even higher affinity than the Glu-Ureas [17]. Nevertheless, their potential for human imaging of PCa has not been tested. ^{68}Ga is a radionuclide for PET with a half-life of 68 min, highly suitable for clinical imaging given the wide availability of ^{68}Ge/^{68}Ga generators and near-term availability of cyclotron production of this radionuclide [18]. Metal chelators, such as 1,4,7,10-tetraazacyclododecane-1,4,7,10-tetraacetic acid (DOTA), can be efficiently labeled with ^{68}Ga(III) ion. One limitation of ^{68}Ga-labled probes of PSMA is their urinary excretion in the ureters and the bladder, which limits detection of local or local recurrence in the prostate. Due to hepatobiliary excretion, the bladder uptake of [^{18}F]PSMA-1007 could be effectively reduced, but it may potentially lead to an increase in abdominal radioactive background. We hypothesized that the switch of one carboxylate to more hydrophilic oxalate in the ODAP-Urea ligand could potentially enhance its water solubility, resulting in a faster clearance of the radiopharmaceutical from non-target organs. We designed twelve ligands with a variety of linkers between ODAP-Urea and DOTA (P**136**-P**144** in Fig. 1). One radioligand, [^{68}Ga]Ga-P**137**, showing the best preclinical characteristics, was selected for a pilot PET imaging study in three patients, in a head-to-head comparison with the Glu-Urea-based ligand [^{68}Ga]Ga-PSMA-617.

Material and methods

Chemical synthesis

PSMA-targeted ligands P**117**-P**144** were generated using solid phase synthesis and purified by high-performance liquid chromatography (HPLC) to reach > 95% purity. The procedures, purification, and characterization are described in the Supporting Information.

NAALADase assay

PSMA inhibitory activity was determined using a slightly modified method of the fluorescence-based Amplex Red glutamic acid assay [16]. In the presence of 8 μM N-acetylaspartylglutamate (NAAG), lysates of LNCaP cell extracts were incubated with the ligand (variable concentration covering 0.001 nM to 10 μM) for 120 min. The glutamate concentration was measured by incubating with a working solution (50 μL) of the Amplex Red glutamic acid kit for 30 min, and the fluorescence was measured with a plate reader (SYNERGY H1 microplate reader, BioTek, VT, USA) with excitation at 530 nm and emission at 590 nm. Enzyme inhibitory constants (K_i values) were generated using the Cheng-Prusoff conversion. Assays were performed in triplicate. Data analysis was performed using GraphPad Prism version 7.00 for Windows (GraphPad Software, San Diego, CA, USA).

Radiolabeling

[^{68}Ga]$GaCl_3$ was obtained from a ^{68}Ge/^{68}Ga generator (maximum production 1.85 GBq, ITG, Germany). [^{68}Ga]Ga-PSMA-617 and [^{68}Ga]Ga-P**117**-[^{68}Ga]Ga-P**144** were synthesized following a standard procedure [19]. The procedures and yields are described in the Supporting Information.

Stability and solubility studies

The partition coefficients (Log *P*) were determined in phosphate-buffered saline (0.1 M, pH = 7.4)/1-octanol (v/v = 1:1). In a 15-mL centrifuge tube, 0.1 mL of ^{68}Ga-labeled compound (37–74 KBq), 1.9 mL PBS, and 2.0 mL 1-octanol were mixed. The mixture was vortexed for 1 min and then centrifuged at 5000 rpm for 3 min. Three samples (100 μL) from each layer were measured using a gamma counter (Hidex AMG, Sheffield, UK). The experiment was performed in triplicate. The partition coefficient was calculated as the average counts in 1-octanol divided by the average counts in PBS, and the value was expressed as log $P \pm$ SD. To evaluate the stabilities of radioligands in vitro, each ^{68}Ga-labeled compound was incubated in saline at room temperature or in 5% human serum albumin (HSA) at 37 °C for 4 h. To evaluate the stability of potential compound [^{68}Ga]Ga-P**137** in vivo, 500 μL of [^{68}Ga]Ga-P**137** (74 MBq) was injected into a mouse bearing a 22Rv1 tumor via tail vein. After 30 min, the mouse was sacrificed, and the urine and serum were collected. The kidneys and liver were added to 5-mL centrifuge tubes. After the addition of 1 mL acetonitrile, the tissues were homogenized for 5 min and were centrifuged for another 5 min. Supernatant was then

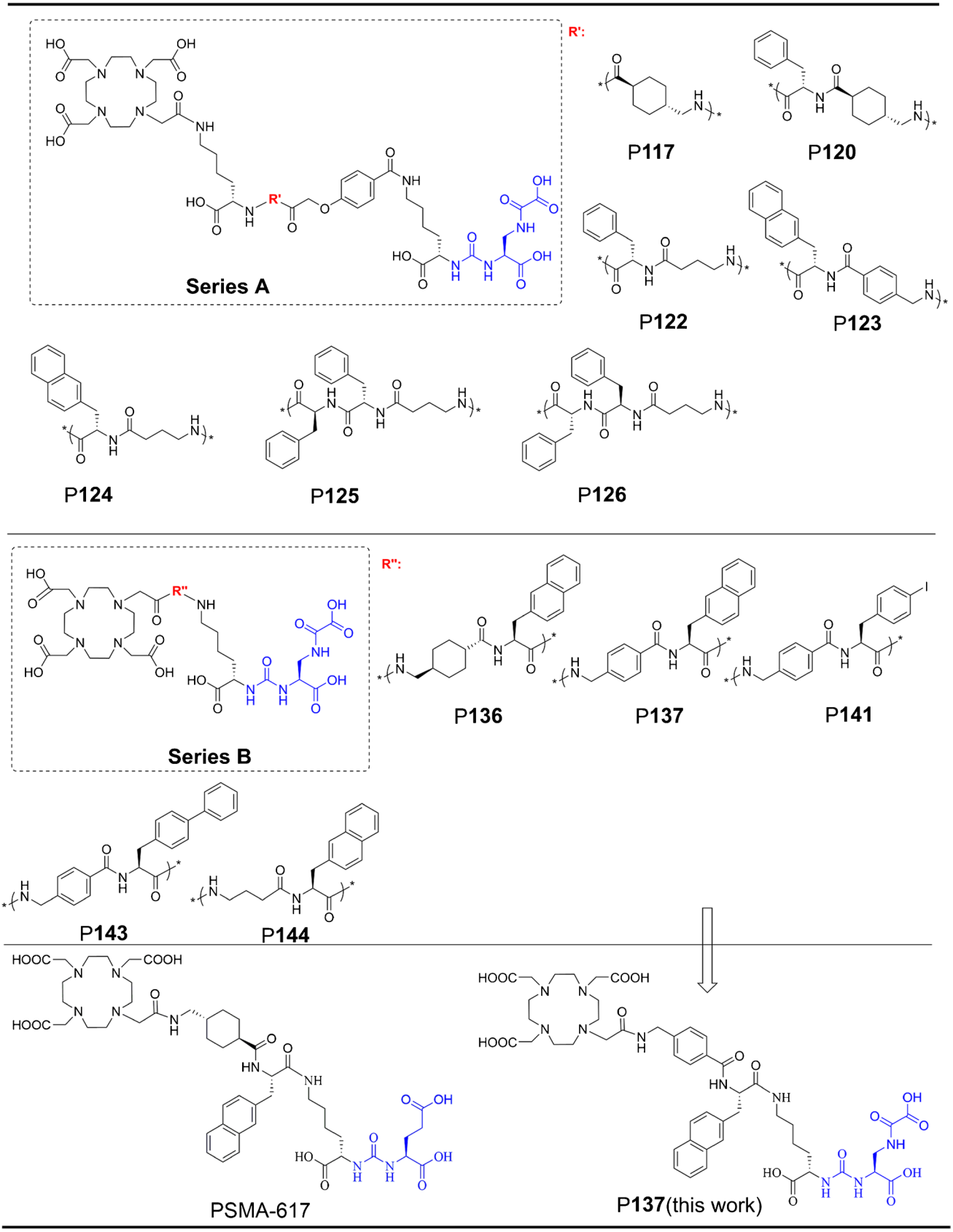

Fig. 1 The chemical structures of ODAP-PSMA ligands and PSMA-617 in this article

collected. After passing the protein-free supernatant through a 0.22-μm filter (Jinteng, Tianjin, China), metabolites and parent compound were measured by radio-HPLC.

Cell lines and mouse models

The human prostate cancer cell lines LNCaP, 22Rv1, and PC3 were obtained from the Chinese Academy of Sciences Typical Culture Collection (Shanghai, China). They were maintained in RPMI 1640 medium containing 10% fetal bovine serum (FBS), 1% penicillin–streptomycin, and 1% GlutaMax-I, under a 5% CO_2-humidified atmosphere at 37 °C. Animal studies were carried out in compliance with the regulations on the use of laboratory animals of the Beijing municipality (Animal Ethics Approval Number: 202019). Four- to 6-week-old male BALB/c nude mice (Charles River, Beijing, China) were implanted subcutaneously with 22Rv1 (10^7 cells/mouse in PBS) cells at the upper right or left flank. When the tumor reached 500–1000 mm^3, the mice were used for the study.

Cellular uptake studies

A cell uptake study was performed on high PSMA-expressing LNCaP, medium PSMA-expressing 22Rv1, and low PSMA-expressing PC-3 cell lines. Cells (10^5 cells/well) were seeded in 24-well plates coated by poly-L-lysine (Sigma, MO, USA) and were incubated for 48 h before the experiments. The medium was removed, and the cells were washed once with fresh medium. The cells in each well were treated with RPMI 1640 medium containing 24 nmol/L radioligand (6.17–12.34 GBq/μmol) at 37 °C for 1 h. After the medium was removed, the cells were washed twice with cold PBS (0.2% BSA, 2 × 0.5 mL). Then, the cells were incubated twice with 0.5 mL of glycine–HCl (50 mM, pH = 2.8) for 5 min to remove the surface-bound fraction; the supernatant was collected. The cells were lysed with 0.5 mL NaOH (0.5 M) and collected. The quantification of binding activity was performed on a γ-counter. For the blocking study, 10 μmol/L of a potent PSMA inhibitor (ZJ-43) was added before the cells were treated with 24 nmol/L of ^{68}Ga-labeled ligand.

MicroPET imaging studies and biodistribution

Before the start of the experiments, all animals were kept in an SPF (specific pathogen-free) environment. During experiments, mice were randomly divided into groups, and four in each group. Male BALB/c nude mice-bearing 22Rv1 tumors (500–1000 mm^3) were injected with [^{68}Ga]Ga-labeled ligands (5.6–7.4 MBq, 100–150 μL, 0.8–1.2 nmol) via the tail vein. For the blocking group, ZJ-43 (50 mg/kg, approximately 3286 nmol calculated by 20 g per mouse) was injected 30 min before the radiotracer injection. Mice were anesthetized (2% sevoflurane) and placed into a PET scanner (Super-Nova®, PINGSHENG, Shanghai, China). PET/CT imaging was performed at 60-min post-injection for a static scan and performed at 0- to 60-min post-injection for a dynamic scan. The images were iteratively reconstructed applying median root prior correction and were converted to standardized uptake value (SUV) images. For organ distribution studies, the [^{68}Ga]Ga-P**137** (0.1 mL, 0.74 MBq) was injected via tail vein to mice-bearing 22Rv1 tumors. The animals were sacrificed at 30-min, 1-h, and 2-h post-injection. Organs of interest were dissected, blotted, and weighed. The radioactivity was measured using a γ-counter and calculated as the percentage uptake of injected activity per gram of tissue (%IA/g). For the blocking experiment, ZJ-43 was injected into animals (50 mg/kg) 30 min before the [^{68}Ga]Ga-P**137** was injected.

Human PET/CT study

To study the radioactive uptake of [^{68}Ga]Ga-P**137** in the lesion sites of PCa patients and evaluate the ability of [^{68}Ga]Ga-P**137** to detect PSMA overexpression in PCa patients. A pilot PET imaging study in PCa patients was carried out from September 2020, and the further clinical studies are still ongoing. This study was approved by the Medical Ethics Committee of Peking University Cancer Hospital and Institute in accordance with national regulations in China and the Helsinki Declaration (ethical approval no. 2020 KT107), and oral and written informed consent was obtained from all participants. [^{68}Ga]Ga-P**137** and [^{68}Ga]Ga-PSMA-617 used in this clinical study reached all quality control standards with radiochemical purity > 99%. The mean and standard deviation of the administered mass of [^{68}Ga]Ga-P**137** was 6.8 ± 1.4 μg (range, 5.7-8.4 μg). The mean administered activity was 128 ± 26 MBq (range, 107-158 MBq). There were no adverse or clinically detectable pharmacologic effects in any of the subjects. No significant changes in vital signs or the results of laboratory studies or electrocardiograms were observed. For direct comparison, patients underwent [^{68}Ga]Ga-P**137** and [^{68}Ga]Ga-PSMA-617 PET-CT scans within 5 days. No patient received any treatment between [^{68}Ga]Ga-P**137** and [^{68}Ga]Ga-PSMA-617 PET/CT. Each patient received an intravenous injection of [^{68}Ga]Ga-P**137** (128 ± 26 MBq, 6.8 ± 1.4 μg) and [^{68}Ga]Ga-PSMA-617 (156 ± 55 MBq, 4.5 ± 0.93 μg). We encouraged patients to drink 1000 mL of water after injection of the radiotracers and to urinate before PET/CT imaging. Whole-body PET/CT scans were performed at 60-min post-injection on the same scanner. PET/CT imaging was performed on a Biograph mCT flow scanner (Siemens Healthineers, Erlangen, Germany) using FlowMotion mode. ^{68}Ga activity was decay-corrected to the time of injection and normalized

to the total amount of activity administered. An unenhanced CT scan (120 kV, 210 Eff.mAs, CARE Dose 4D, CARE kV; reconstructed with a soft-tissue kernel to a slice thickness of 3 mm) was performed followed by PET acquired in 3D mode with 1 mm/s bed speed using FlowMotion. After random, scatter, and decay corrections, PET raw data were reconstructed with ultra-HD-PET (Siemens Healthineers) using 2 iterations, 21 subsets and 5-mm Gaussian filters, 200 × 200 matrix, and Zoom 1.0. Physiologic normal organ uptake, lesion numbers and lesion uptake were compared.

Results

Chemical synthesis and PSMA inhibition potencies

P**117**-P**144** could be efficiently synthesized via solid phase and obtained with moderate yield (12.1-44.4%) and high purity (> 95%) after HPLC purification. The final products are confirmed by mass spectrometry, shown in the Supporting Information (Table S1). Binding affinities are shown in Table 1. All ligands showed low nanomolar affinity to PSMA, which proved the potential for ODAP-Urea-based ligands as a general targeting moiety to PSMA [17]. Ligands with aromatic acids conjugated to ODAP-Urea-Lys (P**136**-P**144**, K_i = 0.13-0.43 nM) demonstrated higher affinity to PSMA than did those with alkoxybenzoic acids (P**117**-P**126**, K_i = 1.12-5.47 nM). That observation is consistent with the structure–activity relationships reported for Glu-Urea-Lys ligands in the S1 sub-binding domain of PSMA [12, 19]. P**137** showed a higher affinity than other aromatic amino acids conjugated ODAP-Urea-Lys with a K_i of 0.13 nM, which is similar to PSMA-617 with a K_i of 0.16 nM.

Radiolabeling

After optimization, ^{68}Ga radiolabeling was reproducibly performed with over 90% radiochemical yield by heating 370-629 MBq $^{68}Ga^{3+}$ with the ligand in pH 4-5 NaOAc buffer at 85-90 °C for 10 min. After purification by Sep-Pak® Light C18 cartridge, radiopharmaceutical was obtained and used for the screening and preclinical and translational (human) studies (Table S2).

Table 1 PSMA inhibition potency of the ligands

Ligand	K_i (nM)	95%CT[a]	Ligand	K_i (nM)	95%CT[a]
P**117**	1.29	0.18-9.75	P**136**	0.37	0.22-0.61
P**120**	1.12	0.53-2.44	P**137**	0.13	0.06-0.32
P**122**	1.12	0.44-3.09	P**141**	0.43	0.17-0.98
P**123**	5.47	3.32-8.93	P**143**	0.22	0.05-0.96
P**124**	4.37	1.70-11.02	P**144**	0.22	0.12-0.43
P**125**	5.34	3.19-8.64	PSMA-617	0.16	0.10-0.24
P**126**	4.89	2.88-8.11			

[a]Confidence interval

Stability and solubility studies of ^{68}Ga-labeled ODAP-PSMA compounds

The stabilities of radioligands were evaluated in vitro. As shown in Fig. S6, all the ^{68}Ga-labeled ODAP-PSMA compounds are stable within 4 h in saline and in 5% HSA. Potential compound [^{68}Ga]Ga-P**137** was also stable in the mice as analyzed for tumor, blood, kidney, and urine at 30-min post-injection. All the ^{68}Ga-labeled ODAP-PSMA compounds were hydrophilic (Table S2). The log *P* value of potential compound [^{68}Ga]Ga-P**137** was − 2.48 ± 0.18, indicating it is more hydrophilic than [^{68}Ga]Ga-PSMA-617 (− 2.00 ± 0.27).

Cell uptake studies

In LNCaP cells, [^{68}Ga]Ga-P**123** has the highest internalization fraction (71.2 ± 1.76%), but its cell uptake value was not high. [^{68}Ga]Ga-P**137** showed the excellent characteristics: the highest uptake value (2.97 ± 0.18% IA/10^5 cells) and the same internalization fraction as [^{68}Ga]Ga-PSMA-617 (66.2 ± 2.51% vs 66.2 ± 2.57%) (Table S3, Fig. 2). [^{68}Ga]Ga-P**137** showed significantly higher uptake in other PSMA-positive cell (22Rv1) than in PSMA-negative cells (PC3), which could be blocked by the known PSMA inhibitor ZJ-43 [20] (Fig. 2).

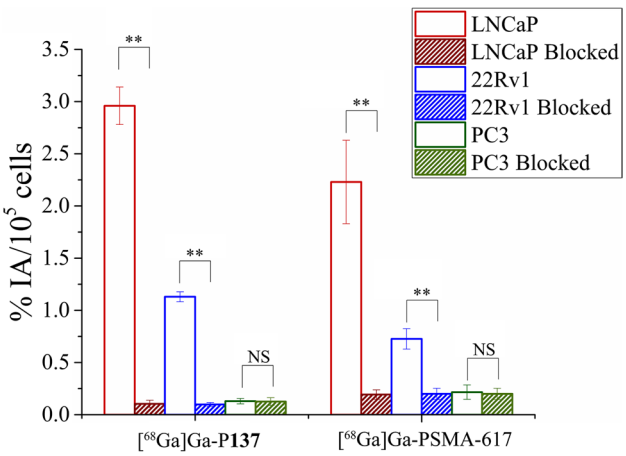

Fig. 2 The radioactivity uptake of [^{68}Ga]Ga-P**137** in LNCaP, 22Rv1 and PC3 compared with [^{68}Ga]Ga-PSMA-617. $^{**}P < 0.01$, NS = not statistically significant

In vivo screening

Following the general procedures for microPET imaging, 5.6-11.1 MBq of freshly labeled [^{68}Ga]Ga-P**117-144** was injected into male BALB/c nude mice-bearing 22Rv1 tumors (n = 4 for each group) and evaluated by PET static imaging at 60-min post-injection. The SUV_{max} of tumor, muscle, and kidneys is collected and compared with [^{68}Ga]Ga-PSMA-617 as shown in Table 2. [^{68}Ga]Ga-PSMA-617 showed high tumor uptake and suitable pharmacokinetics, in keeping with prior reports [12]. Screening showed that [^{68}Ga]Ga-**P137** demonstrated pharmacokinetic properties superior to those of the other ODAP-Urea-based ligands and were similar to those of [^{68}Ga]Ga-PSMA-617. For example, the tumor/muscle ratio for [^{68}Ga]Ga-**P137** was 7.16 ± 2.78, while that for [^{68}Ga]Ga-PSMA-617 was 7.20 ± 2.31. The tumor/kidney ratios were 1.09 ± 0.41 and 1.20 ± 0.39, respectively. Meanwhile, the absolute tumor uptake of [^{68}Ga]Ga-**P137** was 1.45-fold higher than that of [^{68}Ga]Ga-PSMA-617 (0.48 ± 0.27 vs 0.33 ± 0.18). That initial result encouraged us to carry out further studies of [^{68}Ga]Ga-P**137**.

Biodistribution of [^{68}Ga]Ga-P137

To determine the organ distribution of [^{68}Ga]Ga-P**137**, we carried out a biodistribution study in mice-bearing 22Rv1 tumors at 30 min, 1 h, and 2 h. At 1-h post-injection, a blocking group (pre-injection with competitive inhibitor, ZJ-43) and [^{68}Ga]Ga-PSMA-617 imaging group were also conducted as controls. Results are shown in Fig. 3 and Table S4. Tumor and kidney uptake of [^{68}Ga]Ga-P**137** was the highest among the organs tested at 30 min, 1 h, and 2 h (tumor: 5.69 ± 1.11, 6.43 ± 0.98, 6.91 ± 2.07%IA/g; kidney: 26.00 ± 17.86, 6.04 ± 2.16, 3.57 ± 1.03%IA/g) (Fig. 3a), which was blocked by pre-injection of ZJ-43 (tumor: 1.13 ± 0.33%IA/g; kidney: 1.77 ± 0.68%IA/g). [^{68}Ga]

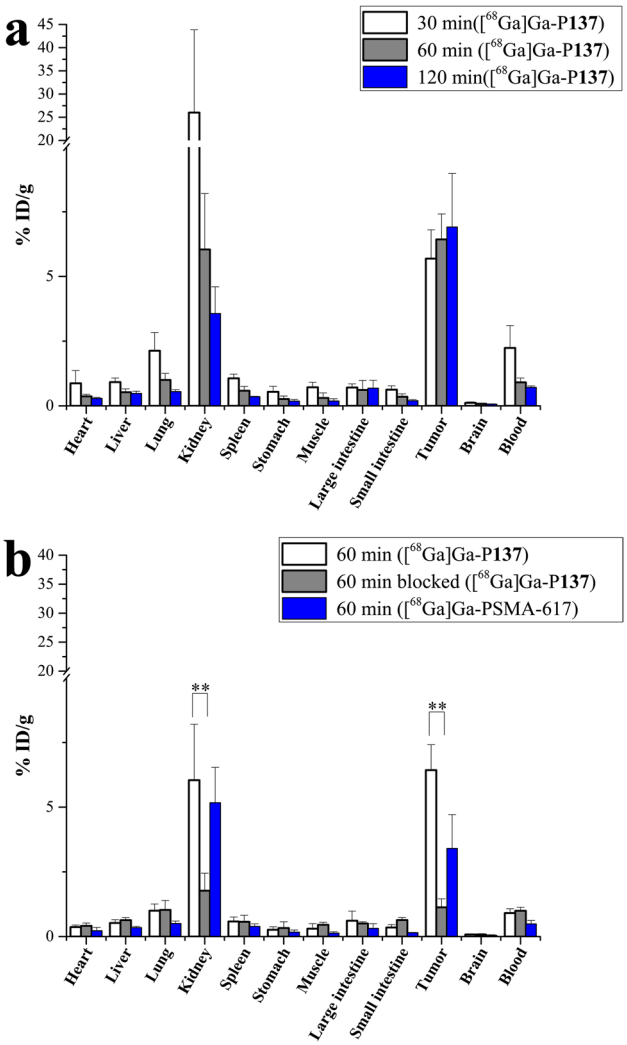

Fig. 3 Organ distribution of [^{68}Ga]Ga-P**137** at 30 min, 60 min and 120 min post-injection (**a**) and blocking experiment at 60-min post-injection (**b**). Data are %IA/g of tissue ± SD (n = 4)

Table 2 SUV values for tumor, muscle, and the kidneys from microPET imaging at 60-min post-injection (mean ± SD, n = 4)

SUVmax	Tumor	Muscle	Kidney	T/M	T/K
[^{68}Ga]Ga-PSMA-617	0.33 ± 0.18	0.06 ± 0.01	0.33 ± 0.07	7.20 ± 2.31	1.20 ± 0.39
[^{68}Ga]Ga-P**117**	0.13 ± 0.05	0.03 ± 0.01	0.32 ± 0.09	4.38 ± 0.93	0.41 ± 0.07
[^{68}Ga]Ga-P**120**	0.19 ± 0.09	0.06 ± 0.02	0.54 ± 0.24	3.71 ± 2.25	0.38 ± 0.14
[^{68}Ga]Ga-P**122**	0.18 ± 0.10	0.05 ± 0.02	0.69 ± 0.36	3.21 ± 1.38	0.26 ± 0.11
[^{68}Ga]Ga-P**123**	0.41 ± 0.05	0.16 ± 0.07	6.94 ± 2.37	3.01 ± 1.48	0.06 ± 0.02
[^{68}Ga]Ga-P**124**	0.34 ± 0.08	0.09 ± 0.01	1.37 ± 0.27	3.85 ± 0.46	0.25 ± 0.03
[^{68}Ga]Ga-P**125**	0.20 ± 0.03	0.08 ± 0.01	1.61 ± 0.33	2.62 ± 0.39	0.13 ± 0.05
[^{68}Ga]Ga-P**126**	0.21 ± 0.02	0.05 ± 0.01	1.05 ± 0.10	3.89 ± 0.28	0.20 ± 0.03
[^{68}Ga]Ga-P**136**	0.23 ± 0.13	0.08 ± 0.03	0.31 ± 0.09	3.28 ± 1.22	0.76 ± 0.20
[^{68}Ga]Ga-P**137**	0.48 ± 0.27	0.08 ± 0.01	0.49 ± 0.26	7.16 ± 2.78	1.09 ± 0.41
[^{68}Ga]Ga-P**141**	0.39 ± 0.23	0.08 ± 0.04	0.79 ± 0.53	4.73 ± 0.46	0.50 ± 0.08
[^{68}Ga]Ga-P**143**	0.25 ± 0.05	0.09 ± 0.06	0.66 ± 0.08	3.78 ± 2.34	0.38 ± 0.11
[^{68}Ga]Ga-P**144**	0.29 ± 0.01	0.06 ± 0.01	1.14 ± 0.36	4.83 ± 0.32	0.34 ± 0.08

Ga-P**137** uptake in 22Rv1 tumors increased over the first 2 h, while the uptake in all other organs decreased. Tumor-to-kidney ratios increased over the time, with medium level PSMA-expressing 22Rv1 tumors showing higher radiotracer uptake than kidney after 1 h (tumor-to-kidney ratio: 0.47 ± 0.38 at 30 min, 1.12 ± 0.26 at 1 h, and 1.93 ± 0.24 at 2 h). Compared with [^{68}Ga]Ga-PSMA-617 at 1 h, [^{68}Ga]Ga-P**137** showed higher tumor uptake (6.43 ± 0.98 vs 3.41 ± 1.31%IA/g) (Fig. 3b) and similar tumor-to-background ratios (tumor-to-blood 6.73 ± 1.48 vs 6.97 ± 2.24, tumor-to-muscle 26.97 ± 13.39 vs 29.61 ± 14.54) (Table S1). Overall, the biodistribution results were consistent with the imaging results, suggesting that [^{68}Ga]Ga-P**137** showed similar pharmacokinetic properties to [^{68}Ga]Ga-PSMA-617, with improvement of the tumor uptake to some extent, which suggested clinical translation potential of [^{68}Ga]Ga-P**137**.

Dynamic microPET/CT imaging studies of [^{68}Ga]Ga-P137

We evaluated the dynamic imaging characteristics of [^{68}Ga]Ga-**P137** in a 22Rv1 tumor mouse to further confirm the biodistribution results. For the dynamic scan, microPET/CT imaging was performed every 5 min for 60-min post-injection. The radioactivity uptake in tumor kept increasing and reached its plateau at around 30 min, while the background signal in muscle reached its peak before the first imaging at 5 min and kept decreasing over the first hour (Fig. 4a). The signal uptake in other organs, including kidney, also rapidly cleared and resulted in an increase in tumor contrast over the time (Fig. 4b). The images at selected time points are shown in Fig. 4c. Results agree with the data observed from biodistribution.

Translational PET/CT imaging

Three patients with histologically proven or metastatic PCa were recruited to this study. Their PET scans are shown in Fig. 5. Normal organ biodistribution was similar for both radiotracers, showing uptake in the salivary and lacrimal glands, the small intestine, the liver, the spleen, and the kidneys, while [^{68}Ga]Ga-P**137** demonstrated much lower uptake in the urinary tract than [^{68}Ga]Ga-PSMA-617 ([^{68}Ga]Ga-P**137**/[^{68}Ga]Ga-PSMA-617 SUVmax ratio of 0.20 ± 0.07) (Fig. 5 and Table S5). Both [^{68}Ga]Ga-P**137** and [^{68}Ga]Ga-PSMA-617 PET/CT demonstrated moderate-to-high activity uptake in the primary tumor (patient 1 with one primary lesion, SUVmax ([^{68}Ga]Ga-P**137**) vs SUVmax ([^{68}Ga]Ga-PSMA-617): 9.1 vs 11.1, the PET/CT fusion imaging was shown in Fig. 6), multiple lymph node (patient 2 with five lymph node detected, SUVmax ([^{68}Ga]Ga-P**137**) vs SUVmax ([^{68}Ga]Ga-PSMA-617): 12.2 vs 14.5; 13.2 vs 19.3; 28.5 vs 31.0; 22.6 vs 30.1; 13.1 vs 19.1), and bone metastases (patient 3 with one primary lesion and two bone

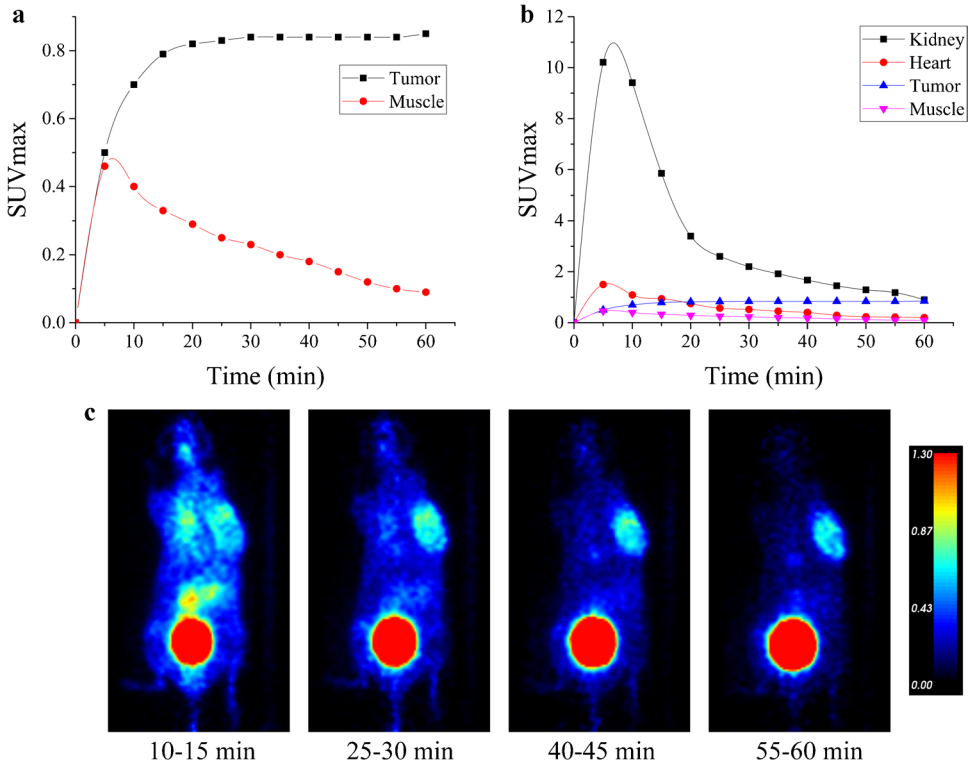

Fig. 4 Time-activity-curves for tumor and muscle (**a**) and for relevant organs (**b**) up to 60-min post-injection of [^{68}Ga]Ga-P**137**. Whole-body coronal slices from microPET imaging of BALB/c nu mouse-bearing 22Rv1 tumor xenografts (**c**). Data are mean standardized uptake value (SUVmean)

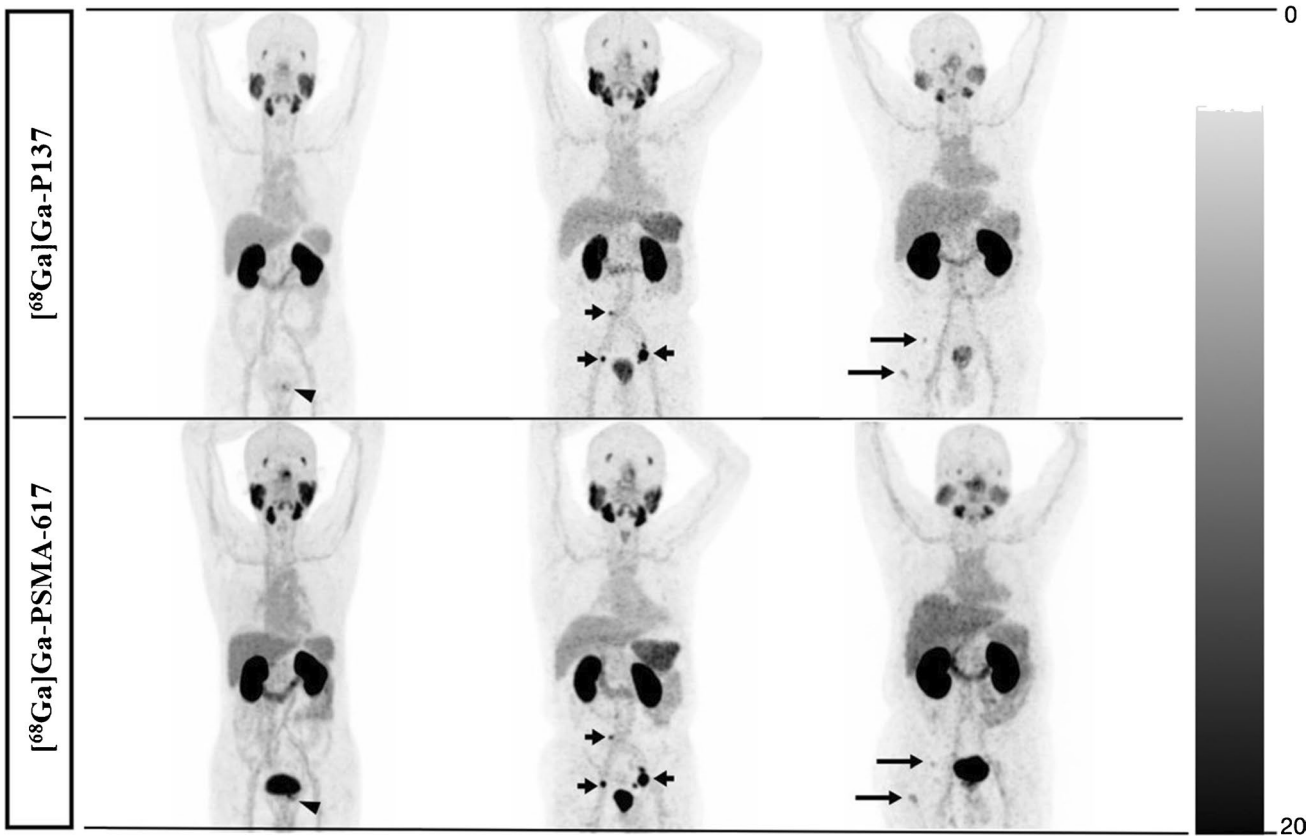

Fig. 5 Comparison of whole-body maximum-intensity projections in three representative patients (patients 1 to 3 from left to right). Physiologic uptake was observed in the salivary and lacrimal glands, the small intestine, the liver, the spleen, and the kidneys for both [^{68}Ga]Ga-P**137** (top) and [^{68}Ga]Ga-PSMA-617 (bottom) maximum intensity projections. In patient 1, [^{68}Ga]Ga-P**137** depicted clearer intraprostatic tumor lesions (arrowhead) than [^{68}Ga]Ga-PSMA-617, with lower bladder background. In patient 2 and patient 3, both radiotracers showed specific retention in multiple lymph node (short arrows) and bone metastases (long arrows)

metastases, SUVmax ([^{68}Ga]Ga-P**137**) vs SUVmax ([^{68}Ga]Ga-PSMA-617): 12.4 vs 10.8; 6.3 vs 3.9; 6.2 vs 4.8).

Discussion

We initiated this study to investigate the feasibility for developing PSMA-targeting radiopharmaceuticals based on the ODAP-Urea scaffold. [^{68}Ga]Ga-DOTA-labeled ligands were first selected for investigation, since their convenient and efficient radiolabeling could accelerate the screening process. Two groups of compounds were synthesized with the targeting moiety (ODAP-Urea-Lys) either conjugated to 4-alkyloxybenzoic acids (P**117**-P**126**) [17] or to aromatic amino acids (P**136**-P**144**) [19]. PSMA binding affinities dictated that the latter group of ligands showed a clear advantage (K_i = 1.12 nM-5.47 nM vs 0.13-0.43 nM, Table 1). The twelve ligands were radiolabeled with ^{68}Ga and evaluated by PET imaging in mice-bearing PSMA-expressing 22Rv1 tumors [21]. The SUV_{max} of tumor, muscle, and kidney indicated [^{68}Ga]Ga-P**137** is superior to other ODAP-Urea ligands tested, but there was no clear difference between the two groups of ligands in both absolute tumor uptake and tumor-to-muscle ratio (Table 2). That might reflect the complicated cell uptake process in vivo. Comparing the side chain of aromatic amino acids ([^{68}Ga]Ga-P**137**, [^{68}Ga]Ga-P**141**, and [^{68}Ga]Ga-P**143**), naphthalenyl showed advantages over substituted phenyl and biphenyl in both tumor uptake and background clearance. The linker between the DOTA chelator and aromatic amino acid also affected pharmacokinetic properties significantly ([^{68}Ga]Ga-P**136**, [^{68}Ga]Ga-P**137**, and [^{68}Ga]Ga-P**144**), with phenyl superior to cyclohexanyl and propyl. After initial screening, [^{68}Ga]Ga-P**137** stood out in both affinity and imaging quality in tumor-bearing mice among the ODAP-ligands tested, which was comparable to [^{68}Ga]Ga-PSMA-617 in potency and pharmacokinetics, with modest increase in absolute tumor uptake.

We carried out further detailed studies of [^{68}Ga]Ga-**P137**. [^{68}Ga]Ga-**P137** was stable in vitro and in vivo. In vitro studies confirmed the specific uptake of PSMA-expressing LNCaP cells and PSMA-expressing 22Rv1 cells (Fig. 2). Under the

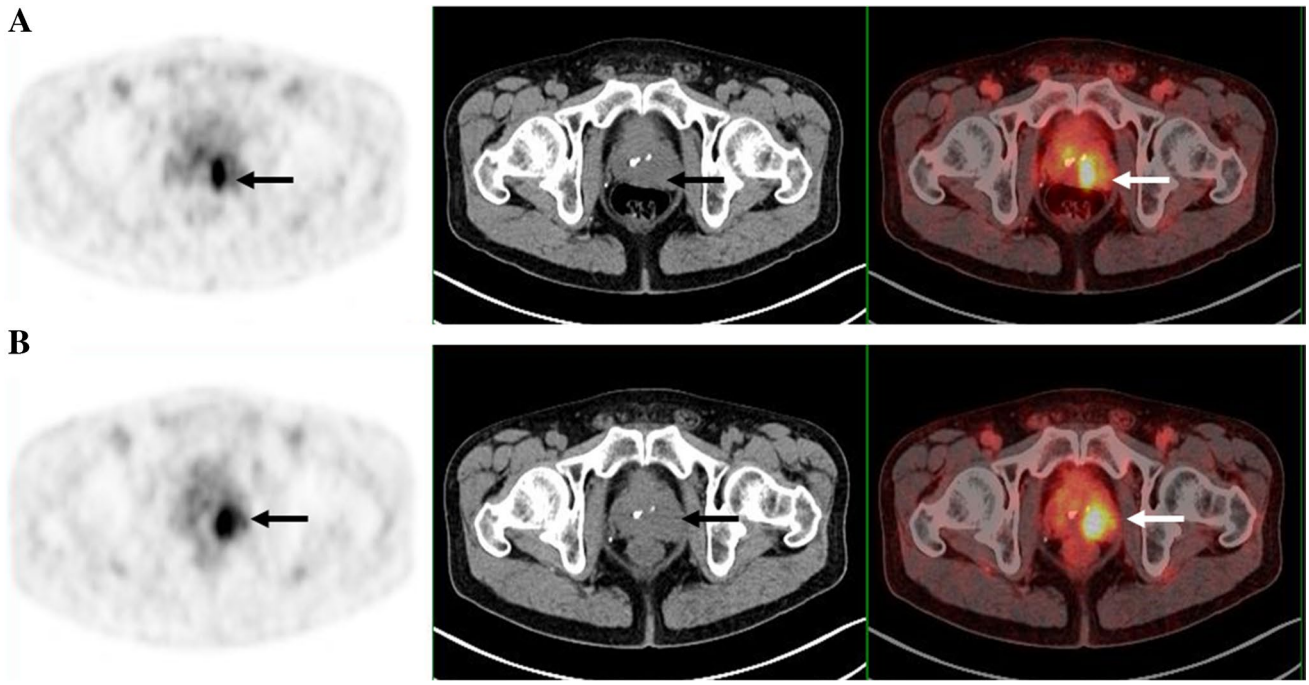

Fig. 6 Images from [^{68}Ga]Ga-P137 PET/CT (**A**) and [^{68}Ga]Ga-PMSA-617 PET/CT (**B**) show intense tracer uptake at primary focus of prostate cancer site(arrow pointed) in patient 1. Left images: PET images. Middle images: axial CT images. Right images: axial-fused PET/CT images

same condition, [^{68}Ga]Ga-P**137** showed 1.3 times higher cell uptake than [^{68}Ga]Ga-PSMA-617 (2.97 ± 0.18%IA/10^5 cells vs 2.23 ± 0.40%IA/10^5 cells) which is in agreement with the observation in the static imaging study at 1 h. Like other successful PSMA imaging agents, tumor and kidney showed the highest initial uptake of radiopharmaceutical in biodistribution studies.

To test the feasibility for clinical imaging, we performed a pilot study in three patients in head-to-head comparison with [^{68}Ga]Ga-PSMA-617. As shown in Fig. 5, radiopharmaceutical uptake is observed in the salivary and lacrimal glands and the kidneys, which is in keeping with Glu-Urea-based ligands. [^{68}Ga]Ga-P**137** identified an intra-prostatic tumor lesion (patient 1), multiple lymph node lesions (patient 2), and bone metastases (patient 3) compared to [^{68}Ga]Ga-PSMA-617. Probably due to higher hydrophilicity (log P: -2.45 ± 0.18 for [^{68}Ga]Ga-P**137** vs -2.00 ± 0.23 for [^{68}Ga]Ga-PSMA-617), [^{68}Ga]Ga-P**137** demonstrated faster clearance and significantly lower uptake in the bladder than [^{68}Ga]Ga-PSMA-617, which may prove advantageous in depicting intra-prostatic lesions. Further study is necessary to confirm and uncover the mechanism for that observation.

Conclusion

ODAP-Urea-based PSMA-targeting ligands can be used to image PSMA in vivo, including in humans. [^{68}Ga]Ga-P**137** demonstrated the most promising characteristics within the series tested, including high PSMA binding affinity, high in vitro and in vivo stability, and high PSMA-specific cell uptake. Compared with [^{68}Ga]Ga-PSMA-617, [^{68}Ga]Ga-P**137** showed better pharmacokinetics with significantly reduced accumulation in the bladder in our pilot clinical study, warranting further investigation of ODAP-Urea-based PSMA-targeting radiopharmaceuticals.

Supplementary Information The online version contains supplementary material available at https://doi.org/10.1007/s00259-021-05486-x.

Acknowledgements We gratefully appreciate all the chemists, nurses, and technicians from the Department of Nuclear Medicine, Peking University Cancer Hospital for their contributions to imaging studies.

Author contribution Xing Yang, Yan Fan, and Zhi Yang conceived and designed the experiments. Xiaojiang Duan and Futao Liu performed the chemical synthesis of the PSMA-targeting ligands. Xiaojiang Duan,

Hua Zhu, and Zhen Cao performed radiosynthesis, binding affinity, cellular experiments, and animal model preparation. Xiaojiang Duan, Xiaojun Zhang, Jinming Zhang, and Zhen Cao performed preclinical imaging experiments. Chen Liu, Hua Zhu, Ya'nan Ren, Xiaoyi Guo, and Xiaojiang Duan performed the clinical translation imaging preparation and experiments. Xing Yang, Xiaojiang Duan, and Xuekang Cai co-wrote the paper. Zhen Xi and Martin G. Pomper helped the data analysis with constructive discussions. All authors discussed the results and commented on manuscript.

Funding This work was supported by the National Natural Science Foundation of China (21877004, 92059101), the Clinical Medicine Plus X—Young Scholars Project of Peking University (PKU2020L-CXQ029), the Wu Jieping Medical Foundation (320.6750.2020–6-25), the Beijing Science and Technology Project (Z181100001618017), and the Science Foundation of Peking University First Hospital (2019SF08), the Found For Fostering Young Scholars of Peking University Health Science Center (BMU2021PYB024) .

Data availability Not applicable.

Code availability Not applicable.

Declarations

Ethics approval All procedures involving human participants were carried out in accordance with the Ethics Committee of Peking University Cancer Hospital (2020KT107) and registered in NIH (NCT04560725). All animal studies were performed according to a protocol approved by the Peking University First Hospital Animal Care and Use Committee.

Informed consent Written informed consents were obtained from all participants included in the study.

Consent to participate Written informed consents were obtained from all participants included in the study.

Consent for publication Not applicable.

Conflict of interest The authors declare no competing interests.

References

1. Siegel RL, Miller KD, Fuchs HE, Jemal A. Cancer statistics, 2021. CA Cancer J Clin. 2021;71:7–33.
2. Bray F, Ferlay J, Soerjomataram I, Siegel RL, Torre LA, Jemal A. Global cancer statistics 2018: GLOBOCAN estimates of incidence and mortality worldwide for 36 cancers in 185 countries. CA Cancer J Clin. 2018;68:394–424.
3. Ross JS, Sheehan CE, Fisher HA, et al. Correlation of primary tumor prostate-specific membrane antigen expression with disease recurrence in prostate cancer. Clin Cancer Res. 2003;9:6357–62.
4. Rowe SP, Gorin MA, Pomper MG. Imaging of prostate-specific membrane antigen with small-molecule PET radiotracers: from the bench to advanced clinical applications. Annu Rev Med. 2019;70:461–77.
5. Sheikhbahaei S, Afshar-Oromieh A, Eiber M, et al. Pearls and pitfalls in clinical interpretation of prostate-specific membrane antigen (PSMA)-targeted PET imaging. Eur J Nucl Med Mol Imaging. 2017;44:2117–36.
6. Von Eyben FE, Picchio M, Von Eyben R, Rhee H, Bauman G. ^{68}Ga-labeled prostate-specific membrane antigen ligand positron emission tomography/computed tomography for prostate cancer: a systematic review and meta-analysis. Eur Urol Focus. 2016;4:686–93.
7. Wester HJ, Schottelius M. PSMA-targeted radiopharmaceuticals for imaging and therapy. Semin Nucl Med. 2019;49:302–12.
8. Mease RC, Dusich CL, Foss CA, et al. N-[N-[(S)-1,3-Dicarboxypropyl]carbamoyl]-4-[^{18}F]fluorobenzyl-L-cysteine, [^{18}F] DCFBC: a new imaging probe for prostate cancer. Clin Cancer Res. 2008;14:3036–43.
9. Chen Y, Pullambhatla M, Foss CA, et al. 2-(3-{1-Carboxy-5-[(6-[^{18}F]fluoro-pyridine-3-carbonyl)-amino]-pentyl}-ureido)-pentanedioic acid, [^{18}F]DCFPyL, a PSMA-based PET imaging agent for prostate cancer. Clin Cancer Res. 2011;17:7645–53.
10. Cardinale J, Schäfer M, Beneˇsová M, et al. Preclinical evaluation of ^{18}F-PSMA-1007, a new prostate-specific membrane antigen ligand for prostate cancer imaging. J Nucl Med. 2017;58:425–31.
11. Eder M, Schafer M, Bauder-Wust U, et al. ^{68}Ga-complex lipophilicity and the targeting property of a urea-based PSMA inhibitor for PET imaging. Bioconjug Chem. 2012;23:688–97.
12. Benešová M, Schäfer M, Bauder-Wüst U, et al. Preclinical evaluation of a tailor-made DOTA-conjugated PSMA inhibitor with optimized linker moiety for imaging and endoradiotherapy of prostate cancer. J Nucl Med. 2015;56:914–20.
13. Kabasakal L, AbuQbeitah M, Aygun A, et al. Pre-therapeutic dosimetry of normal organs and tissues of ^{177}Lu-PSMA-617 prostate-specific membrane antigen (PSMA) inhibitor in patients with castration-resistant prostate cancer. Eur J Nucl Med Mol Imaging. 2015;42:1976–83.
14. Martina W, Margret S, Jakub S, et al. ^{68}Ga- and ^{177}Lu-labeled PSMA I&T: optimization of a PSMA-targeted theranostic concept and first proof-of-concept human studies. J Nucl Med. 2015;56:1169–76.
15. Graham K, Lesche R, Gromov AV, et al. Radiofluorinated derivatives of 2-(phosphonomethyl)pentanedioic acid as inhibitors of prostate specific membrane antigen (PSMA) for the imaging of prostate cancer. J Med Chem. 2012;55:9510–20.
16. Yang X, Mease RC, Pullambhatla M, et al. [^{18}F]Fluorobenzoyllysinepentanedioic acid carbamates: new scaffolds for positron emission tomography (PET) imaging of prostate-specific membrane antigen (PSMA). J Med Chem. 2016;59:206–18.
17. Duan X, Liu F, Kwon H, et al. (S)-3-(Carboxyformamido)-2-(3-(carboxymethyl)ureido)propanoic acid as a novel PSMA targeting scaffold for prostate cancer imaging. J Med Chem. 2020;63:3563–76.
18. Thisgaard H, Kumlin J, Langkjaer N, et al. Multi-curie production of gallium-68 on a biomedical cyclotron and automated radiolabelling of PSMA-11 and DOTATATE. EJNMMI Radiopharm Chem. 2021;6:1–11.
19. Benešová M, Bauderwüst U, Schäfer M, et al. Linker modification strategies to control the prostate-specific membrane antigen (PSMA)-targeting and pharmacokinetic properties of DOTA-conjugated PSMA inhibitors. J Med Chem. 2016;59:1761–75.
20. Olszewski RT, Bukhari N, Zhou J, et al. NAAG peptidase inhibition reduces locomotor activity and some stereotypes in the PCP model of schizophrenia via group II mGluR. J Neurochem. 2004;89:876–85.
21. Liu T, Liu C, Xu X, et al. Preclinical evaluation and pilot clinical study of Al^{18}F-PSMA-BCH for prostate cancer imaging. J Nucl Med. 2019;60:1284–92.

Authors and Affiliations

Xiaojiang Duan[1] · Zhen Cao[1] · Hua Zhu[2] · Chen Liu[2] · Xiaojun Zhang[3] · Jinming Zhang[3] · Ya'nan Ren[2] · Futao Liu[2] · Xuekang Cai[1] · Xiaoyi Guo[2] · Zhen Xi[4] · Martin G. Pomper[5] · Zhi Yang[2] · Yan Fan[1] · Xing Yang[1,6]

Xiaojiang Duan
duanxj@pku.edu.cn

Zhen Cao
1063624342@qq.com

Hua Zhu
zhuhuananjing@163.com

[1] Department of Nuclear Medicine, Peking University First Hospital, Beijing 100034, China

[2] Key Laboratory of Carcinogenesis and Translational Research (Ministry of Education/Beijing), Department of Nuclear Medicine, Peking University Cancer Hospital & Institute, Beijing 100142, China

[3] Department of Nuclear Medicine, the First Medical Center of Chinese PLA General Hospital, Beijing 100853, China

[4] State Key Laboratory of Elemento-Organic Chemistry and Department of Chemical Biology, National Pesticide Engineering Research Center, Nankai University, Tianjin 300071, China

[5] Russell H. Morgan Department of Radiology and Radiological Science, Johns Hopkins Medical Institutions, Baltimore, MD 21287, USA

[6] Institute of Medical Technology, Peking University Health Science Center, Beijing 100191, China